Enhanced decoherence for a neutral particle sliding on a metallic surface in vacuum

Ludmila Viotti, Fernando C. Lombardo, and Paula I. Villar
Departamento de Física Juan José Giambiagi, FCEyN UBA, and IFIBA CONICET-UBA, Facultad de Ciencias Exactas y Naturales, Ciudad Universitaria, Pabellón I, 1428 Buenos Aires, Argentina

(Received 6 November 2020; revised 5 January 2021; accepted 16 February 2021; published 9 March 2021)

Bodies in relative motion, spatially separated in vacuum, experience a tiny friction force known as quantum friction. This force has eluded experimental detection so far due to its small magnitude and short range. Herein, we give quantitative details so as to track traces of the quantum friction by measuring coherences in the atom. We notice that the environmentally induced decoherence can be decomposed into contributions of different signature: corrections induced by the electromagnetic vacuum in the presence of the dielectric sheet and those induced by the motion of the particle. In this direction, we show that noncontact friction enhances the decoherence of the moving atom. Further, its effect can be enlarged by a thorough selection of the two-level particle and the Drude-Lorentz parameters of the material. In this context, we suggest that measuring decoherence times through velocity dependence of coherences could indirectly demonstrate the existence of quantum friction.

DOI: 10.1103/PhysRevA.103.032809

I. INTRODUCTION

Some outstanding features of modern quantum field theory are the nontrivial structure exhibited by the vacuum state and the consequent existence of vacuum fluctuations. These quantum fluctuations induce macroscopic effects over which, in many cases, experimental verification has been achieved and thereafter improved. The most renewed example is the Casimir static force between neutral bodies placed in vacuum [1–8]. Another paradigmatic example is that of the phenomenon known as the dynamical Casimir effect [9–12], in which a mirror moving at time-dependent velocities produces real photons through quantum vacuum fluctuations. However, while experimental observation of these effects has been attained, another phenomenon has eluded experimental detection so far due to its short range and small magnitude. This latter effect consists of the appearance of a dissipative force between spatially separated objects in relative motion, known as quantum friction (QF) [13–18]. This lack of experimental verification favors the coexistence of different theoretical approaches which rely on a variety of assumptions and do not converge to a single result [19]. Such a variety of methods ranges from time-dependent perturbation theory [20,21] and quantum master equations in the Markovian limit [22] to generalized nonequilibrium fluctuation-dissipation relations [23] and thermodynamic principles [24]. There has also been a great deal of theoretical effort devoted to finding favorable conditions for experimental measurements of QF [25–30].

Due to the experimental challenges involved in the implementation of precision measurements for the detection of such a small force on objects near a surface, several works have followed a different approach consisting of tracking traces of quantum friction through the study of velocity-dependent quantum-vacuum effects which could more easily testable. In Refs. [31,32] Volokitin and Persson investigated the van der Waals friction between graphene and an amorphous SiO_2 substrate. They found the electric current to saturate at a high electric field due to this friction. The saturation current depends weakly on the temperature, which they attributed to the quantum friction between the graphene carriers and the substrate optical phonons. They calculated the frictional drag between two graphene sheets caused by van der Waals friction and proved that this drag can induce a voltage high enough to be measured experimentally by state-of-the-art noncontact force microscopy. This work paved the way for the possible mechanical detection of the Casimir friction. In [33] the level shift and decay rate modification arising from the motion of an atom in the presence of a medium were found in the Markovian limit and their relation to the parallel component of vacuum force was discussed. Considering other aspects of the internal dynamics, a toy model for decoherence induced in the state of a particle in motion relative to a material (modeled as set of harmonic oscillators) was studied in [34]. Recently, in [35] some of us examined the effect of the vacuum, dressed by the presence of a more realistic Drude-Lorentz material in the geometric phase acquired by an atom traversing at constant velocity, and made a proposal for an experimental setup.

Following these ideas, in this article we focus on finding an alternative indicator of the existence of quantum friction and explore favorable experimental conditions under which the quantum friction can be detected. Due to the technical issues explained above, we will follow a different approach consisting of tracking traces of quantum friction in the coherences of a two-level system. We will pursue this goal by a thorough study of the decoherence process suffered by a neutral particle in nonrelativistic motion parallel to a metallic surface in an electromagnetic vacuum. In particular, we will try to identify environmentally induced behavior dependent exclusively on the particle's velocity since the mere presence of a velocity contribution in the noise-induced corrections is evidence of

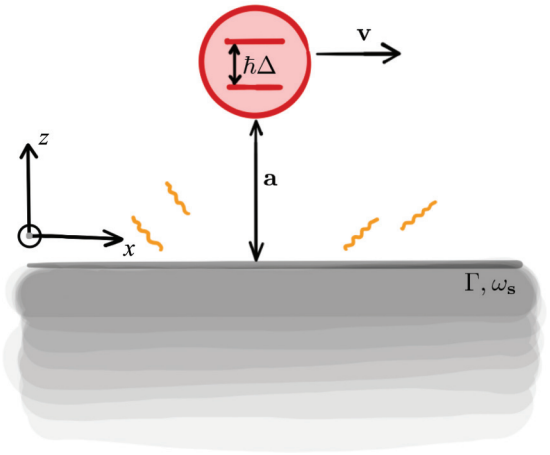

FIG. 1. Scheme of the system under consideration, where the two-level system moves at a fixed distance a from the dielectric plate.

the existence of frictional effect. Environmentally induced decoherence can be decomposed into two contributions: corrections induced by the solely electromagnetic vacuum in the presence of the dielectric sheet and those induced by the motion of the particle. In the end, we aim to prove that the presence of velocity and hence noncontact friction enhances the decoherence of the internal degrees of freedom of the moving atom, suggesting that measuring decoherence times could be used to indirectly demonstrate the existence of quantum friction.

The article is organized as follows. In Sec. II we provide a description of the composite system under investigation. In Sec. III we solve the complete system's dynamics in the nonretarded regime and weak-coupling limit without making either Markovian or low-dissipation approximations. In Sec. IV we present a complete analysis of the environmentally induced dynamics of the system so as to track evidence of quantum-fluctuation-induced effects due to the velocity of the particle, focusing on the conditions under which those effects are enhanced. This research is mainly conducted by observing the suppression of the coherences of the internal degree of freedom of the particle, where this destruction is found to be fastened by the movement of the particle. We further include an analysis of different materials and particles and study how these features impact on the magnitude of the effects under study. In Sec. V we summarize our main conclusions. Two Appendixes complement the work.

II. SYSTEM

Here we consider a neutral particle moving through a medium-assisted electromagnetic field vacuum. As shown in Fig. 1, the particle is modeled as a two-level system whose center of mass follows a prescribed trajectory $\mathbf{r}_s(t) = vt\check{x} + a\check{z}$ at a fixed distance a from a dielectric semi-infinite planar medium. At this point it is worth noting that we have employed the inverted circumflex to denote unit vectors so as to save the circumflex to denote operator nature. The dynamics of the composite system can be described by a Hamiltonian consisting of atomic, field, and interaction contributions defined by

$$\hat{H} = \frac{\hbar}{2}\Delta\hat{\sigma}_z \otimes \mathbb{1} + \hat{H}_{\rm em} + \hat{H}_{\rm int}, \tag{1}$$

where Δ is energy gap of the two-level system and $\hat{H}_{\rm em}$ is the Hamiltonian of the electromagnetic field in the absence of the particle, but in the presence of the dielectric half space at $z < 0$. The interaction between the particle and the field is given in the dipole (long-wavelength) approximation by $\hat{H}_{\rm int} = -\hat{\mathbf{d}} \otimes \hat{\mathbf{E}}(\mathbf{r}_s)$ and depends explicitly on time through the position of the particle, which is treated as a classical variable relying on its uncertainty to be unresolvable by the characteristic wavelength of the electric field. We will restrict ourselves to the nonretarded (near-field) regime where the particle-surface distance a is small enough to satisfy $a\Delta/c \ll 1$. In this regime, the finite time taken for a reflected photon to reach the particle is negligible compared to its natural timescale and the interaction Hamiltonian can therefore be written as $\hat{H}_{\rm int} = \hat{\mathbf{d}} \otimes \nabla\hat{\Phi}(\mathbf{r}_s)$, where the electric potential $\hat{\Phi}$, expanded in a plane-wave basis corresponding to elementary excitations, is [36,37]

$$\hat{\Phi} = \int d^2k \int_0^\infty d\omega[\hat{a}_{\mathbf{k},\omega}, \phi(\mathbf{k},\omega)e^{i\mathbf{k}\cdot\mathbf{r}_\parallel} + \text{H.c.}] \tag{2}$$

and contains all the information of the electric field in the $z > 0$ region, dressed by the dielectric medium. The bosonic operators satisfy the commutation relation $[\hat{a}_{\mathbf{k},\omega}, \hat{a}^\dagger_{\mathbf{k}',\omega'}] = \delta(\mathbf{k} - \mathbf{k}')\delta(\omega - \omega')$ and the single-excitation mode functions are given by

$$\phi(\mathbf{k},\omega) = \sqrt{\frac{\omega\Gamma}{\omega_s}}\sqrt{\frac{\hbar}{2\pi^2 k}}e^{-kz}\frac{\omega_p}{\omega^2 - \omega_s^2 - i\omega\Gamma}, \tag{3}$$

where the wave vector $\mathbf{k} = (k_x, k_y)$ is parallel to the medium surface and $k = |\mathbf{k}|$. The frequency ω_s gives the surface plasmon resonance and the material dissipation rate Γ its broadening while in the Drude model for metals the plasma frequency ω_p satisfies $\omega_p^2 = 2\omega_s^2$.

III. NONUNITARY EVOLUTION OF THE SYSTEM

In order to address the dynamics of the two-level system, we will derive the master equation satisfied by the reduce density matrix representing its state. This is done by integrating out the degrees of freedom corresponding to the composite environment, as indicated by the formalism of open quantum systems [38]. By assuming an initially factorized state $\rho(0) = \rho_s(0) \otimes \rho_{\rm em}^{\rm vac}$ with the dressed electromagnetic field in its vacuum state, the master equation in the interaction picture, up to second order in the coupling constant, is given by [39]

$$\dot{\rho}_s(t) = \frac{-1}{\hbar^2}\int_0^t dt' \text{Tr}_{\rm em}[V(t), [V(t'), \rho_s(t) \otimes \rho_{\rm em}]]. \tag{4}$$

An explicit computation of this expression leads to the equation ruling the temporal evolution of the reduced density matrix [40,41]. In this work we have considered the equation governing the two-level system dynamics that results from performing the secular approximation, also referred to as the post-trace rotating-wave approximation. This approximation consists of neglecting those terms which are fast oscillating

in the interaction picture and it can be performed based on the assumption that dissipative corrections are weak enough to expect to preserve accurate results in the timescales of the phenomena [42,43]. Therefore, the equation we obtain is

$$\begin{aligned}\dot{\rho}_{\rm s} =& -\frac{i\Delta}{2}[\hat{\sigma}_z, \rho_{\rm s}] + i\zeta(v,t)[\sigma_x, \{\sigma_y, \rho_{\rm s}\}] \\ & -\frac{1}{2}D(v,t)([\sigma_x,[\sigma_x,\rho_{\rm s}]]+[\sigma_y,[\sigma_y,\rho_{\rm s}]]) \\ & -\frac{1}{2}f(v,t)([\sigma_x,[\sigma_y,\rho_{\rm s}]]-[\sigma_y,[\sigma_x,\rho_{\rm s}]]),\end{aligned} \tag{5}$$

where the nonunitary effects are modeled by the diffusion coefficients $D(v,t)$ and $f(v,t)$, while dissipative effects are present in $\zeta(v,t)$. All three coefficients consist of real functions of time, with parameters introduced by the particle and the medium-assisted field. These coefficients are developed in Appendix A, where an analytical solution is given for sufficiently low velocities of the particle.

It is important to mention that the diagonal elements of the reduced density matrix are exactly the same whether secular approximation is performed or not, since for this system it only implies disregarding a dynamical interaction between ρ_{12} and ρ_{21}. By resorting to a change of variables, say, $\rho_- = \rho_{11} - \rho_{22}$ and $\rho_+ = \mathrm{Tr}(\rho_{\rm s}) = 1$, a formal solution can easily be found through direct computation,

$$\begin{aligned}\rho_-(t) =& \exp\left(-4\int dt\, D(v,t)\right)\rho_-(0) \\ & -4\exp\left(-4\int dt\, D(v,t)\right)\int_0^t dt'\zeta(v,t') \\ & \times \exp\left(4\int dt' D(v,t')\right).\end{aligned} \tag{6}$$

The nondiagonal elements in this approximation are

$$\begin{aligned}\rho_{12}^{\rm SEC}(t) =& \rho_{12}(0)\exp\left(-\int_0^t dt'[2D(v,t') \right. \\ & \left. +2if(v,t')+i\Delta]\right),\end{aligned} \tag{7}$$

$$\rho_{21}(t) = \rho_{12}^*(t). \tag{8}$$

Hence, after applying the secular approximation, the reduced density matrix describing the state of the particle's internal degree of freedom can be written as $\rho_{\rm s}(t) = \rho_{\rm diag} + \rho_{\rm nond}$, with

$$\rho_{\rm diag} = \begin{pmatrix}\rho_{11}(t) & 0 \\ 0 & 1-\rho_{11}(t)\end{pmatrix} \tag{9}$$

and

$$\begin{aligned}\rho_{\rm nond} =& \begin{pmatrix}0 & \rho_{12}(0)e^{-i\xi(t)} \\ \rho_{12}^*(0)e^{i\xi(t)} & 0\end{pmatrix} \\ & \times \exp\left(-\frac{2}{\omega_{\rm s}}\int_0^t dt' D(v,t')\right),\end{aligned} \tag{10}$$

with

$$\xi(t) = i\tilde{\Delta}t + 2i\int_0^t dt'\frac{f(v,t')}{\omega_{\rm s}}, \tag{11}$$

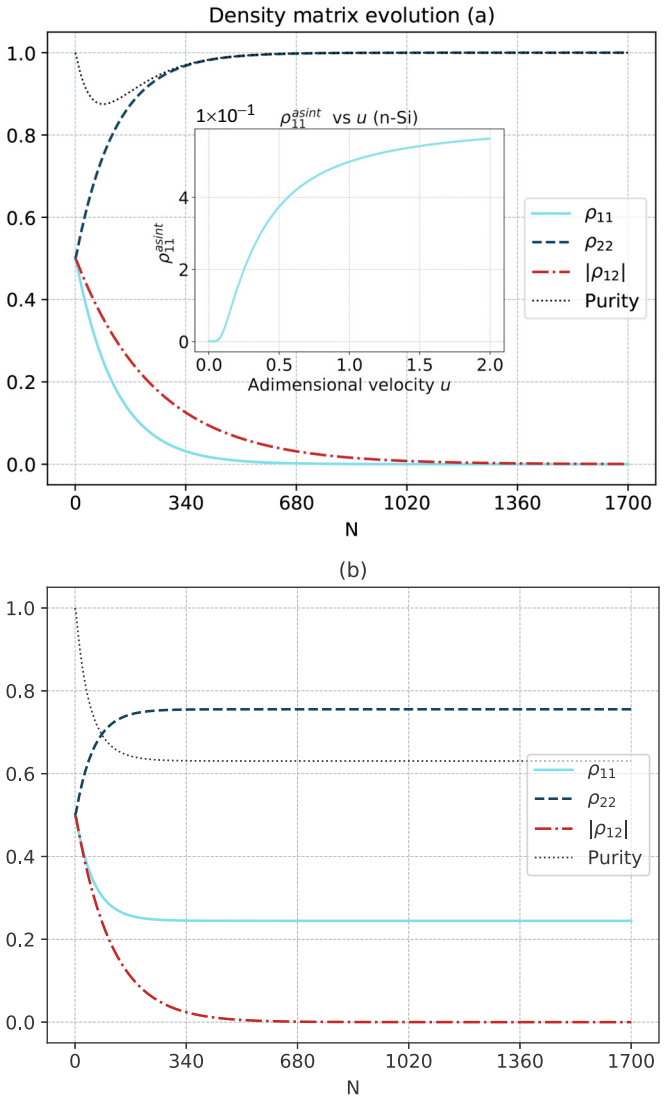

FIG. 2. Matrix elements and purity evolution in natural cycles $N = \frac{t}{2\pi/\tilde{\Delta}}$. (a) The system can be seen to tend to its ground state independently of the initial state for low velocities. (b) For high enough velocity, the asymptotic state is a mixed state. The parameter values are $\tilde{\Gamma} = 1$, $r_0/\omega_{\rm s} = 10^{-2}$, $\tilde{\Delta} = 0.2$, and (a) $u = 0.003$ and (b) $u = 0.3$. The inset in (a) displays the behavior of the asymptotic value of ρ_{11} with dimensionless velocity u.

where we have used the dimensionless parameters $t = \omega_{\rm s}t_{\rm real}$, $u = v/(\omega_{\rm s}a)$, $\tilde{\Gamma} = \Gamma/\omega_{\rm s}$, and $\tilde{\Delta} = \Delta/\omega_{\rm s}$ as defined in Appendix A.

The dynamics of the system can be seen to display two qualitatively different behaviors depending on the velocity of the particle. While for high enough velocities the evolution leads to a mixed asymptotic state, if the velocity is low the system evolves to its ground state. We present both behaviors in Fig. 2. In Fig. 2(a) the particle is considered to move with dimensionless velocity $u = 0.003$. In that case, both the coherences and the ρ_{11} element of the state are indefinitely suppressed and tend to vanish for long enough times, leading the system to its ground state. The purity of the state decreases until reaching a minimal value, from which it starts to recover and finally tends to unity as the system tends to its

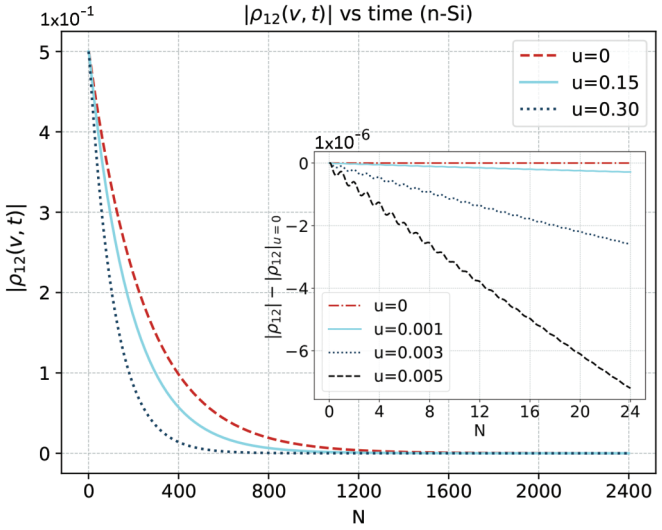

FIG. 3. Coherence evolution, in natural cycles $N = \frac{t}{2\pi/\tilde{\Delta}}$, for different velocity values. The inset shows the difference in the coherence as cycles proceed for smaller velocity values. The parameter values are $\tilde{\Gamma} = 1$, $r_0/\omega_s = 10^{-2}$, and $\tilde{\Delta} = 0.2$.

pure ground state. On the other hand, while the coherences are totally extinguished, for a dimensionless velocity $u = 0.3$ the ρ_{11} element of the reduced density matrix is only suppressed up to an asymptotic value. This behavior, displayed in Fig. 2(b), leads to a mixed asymptotic state whose purity never recovers but lands at a constant value depending on ρ_{11} as $p = \rho_{11}^2 + (1 - \rho_{11})^2$.

The inset in Fig. 2(a) shows the velocity dependence of the asymptotic value of ρ_{11}. The dimensionless velocity $u = \tilde{\Delta}/2$ at which the dynamics of the system acquires a completely different behavior coincides with the lower bound on the velocity, which allows the atom to become excited at the expense of its kinetic energy [44–46]. A few remarks can be made from a more detailed observation of the coherence behaviors. Figure 3 shows off-diagonal elements of the density matrix to be suppressed by the environment. This destruction is seen not only to be fastened by the relative motion between the particle and the material, but also to happen sooner as the velocity is increased; for example, the absolute value of the coherence for a particle in relative motion with $u = 0.3$ becomes extinct sooner than that with $u = 0.15$. The same monotonic behavior is displayed in the inset, in which the difference between absolute values $|\rho_{12}(t)| - |\rho_{12}^{u=0}(t)|$ grows faster as the velocity is increased.

However, as the difference between the value of $|\rho_{12}(t)|$ for finite velocity and that for null velocity attains a maximum value and tends to vanish afterward, explorations of the coherences at too late times would not allow any identification of the velocity-induced effects. As shown in Fig. 2, the same observation would apply to the behavior of both the populations and purity measurements for low velocities as all these converge to a given value for long enough times, independently of the velocity. For high velocities, however, the velocity effect could be observed at late times on the populations or purity measurements, while the coherences will always be completely destroyed if one waits too long.

In the following, we will use the results obtained herein for the reduced density matrix so as to define a scale in which coherences in the internal degree of freedom of the atom are destroyed by the influence of the electromagnetic field dressed by the metallic material.

IV. ENVIRONMENTALLY INDUCED DESTRUCTION OF COHERENCES

In this section we focus on the environmentally induced destruction of the particle's quantum coherences and define a characteristic time in which the process takes place. The density matrix defined by Eqs. (9) and (10) allows us to define a decoherence timescale τ_D from the decoherence function $\mathcal{D}(t) = \exp[-\frac{2}{\omega_s}\int_0^t dt' D(v, t')]$ as $\mathcal{D}(\tau_D) = e^{-2}$.

For low velocities, up to second order in the dimensionless velocity u, this decoherence timescale behaves as

$$\tau_D = \tau_D^{\text{Markov}} + \left[\frac{-1}{\sqrt{4-\tilde{\Gamma}^2}}\frac{g(\tilde{\Delta},\tilde{\Gamma})}{h(\tilde{\Delta},\tilde{\Gamma})} + \frac{2}{\pi\tilde{\Delta}}\right] + \frac{3}{8}\frac{d^{(a)}}{d^{(i)}}u^2\left\{\left[g(\tilde{\Delta},\tilde{\Gamma})\frac{\partial_{\tilde{\Delta}}^2 h(\tilde{\Delta},\tilde{\Gamma})}{h^2(\tilde{\Delta},\tilde{\Gamma})} - \frac{\partial_{\tilde{\Delta}}^2 g(\tilde{\Delta},\tilde{\Gamma})}{h(\tilde{\Delta},\tilde{\Gamma})}\right] + \frac{2}{\pi h(\tilde{\Delta},\tilde{\Gamma})}\left[\partial_{\tilde{\Delta}}^2\frac{h(\tilde{\Delta},\tilde{\Gamma})}{\tilde{\Delta}} - \frac{\partial_{\tilde{\Delta}}^2 h(\tilde{\Delta},\tilde{\Gamma})}{\tilde{\Delta}}\right]\right\}, \quad (12)$$

where the term corresponding to the Markovian approximation can be expressed as

$$\tau_D^{\text{Markov}} = \frac{\hbar\omega_s^2 a^3}{d^2\omega_p^2}\frac{32}{d^{(i)}}\left(\frac{1}{h(\tilde{\Delta},\tilde{\Gamma})} - \frac{3}{8}\frac{d^{(a)}}{d^{(i)}}u^2\frac{\partial_{\tilde{\Delta}}^2 h(\tilde{\Delta},\tilde{\Gamma})}{h^2(\tilde{\Delta},\tilde{\Gamma})}\right). \quad (13)$$

The functions $h(\tilde{\Delta},\tilde{\Gamma})$ and $g(\tilde{\Delta},\tilde{\Gamma})$ appearing in these expressions are defined by

$$h(\tilde{\Delta},\tilde{\Gamma}) = \frac{\tilde{\Delta}\tilde{\Gamma}}{(\tilde{\Delta}^2-1)^2 + \tilde{\Delta}\tilde{\Gamma}},$$
$$g(\tilde{\Delta},\tilde{\Gamma}) = \text{Re}\left[\left(1 + \frac{2i}{\pi}\ln(\tilde{\omega}_r/\tilde{\Delta})\right) \times \left(\frac{1}{(\tilde{\omega}_r+\tilde{\Delta})^2} + \frac{1}{(\tilde{\omega}_r-\tilde{\Delta})^2}\right)\right], \quad (14)$$

with $\tilde{\omega}_r$ as defined in Eq. (A8) and the dependence on the polarization orientation encoded in $d^{(i)}$ and $d^{(a)}$ as defined after Eq. (A11). The dependence of the dynamics on the velocity of the particle (which is already evident in the behavior displayed in Figs. 2 and 3) can therefore be studied by the use of the decoherence time τ_D, which happens to scale as u^2 for low velocities, as seen from Eqs. (12) and (13). This quadratic behavior of the internal dynamics is in agreement with the results found in [33], where among other aspects of the internal dynamics of an atom the decay rate, which is proportional to the Markovian limit of $D(v, t)$, is found to scale as u^2. A similar dependence on u was found in [35] for the corrections induced by the noncontact friction force on the accumulated geometric phase.

Decoherence time being approximated by $\tau_D \sim a - bu^2$ reveals that the effect of the environment on the particle

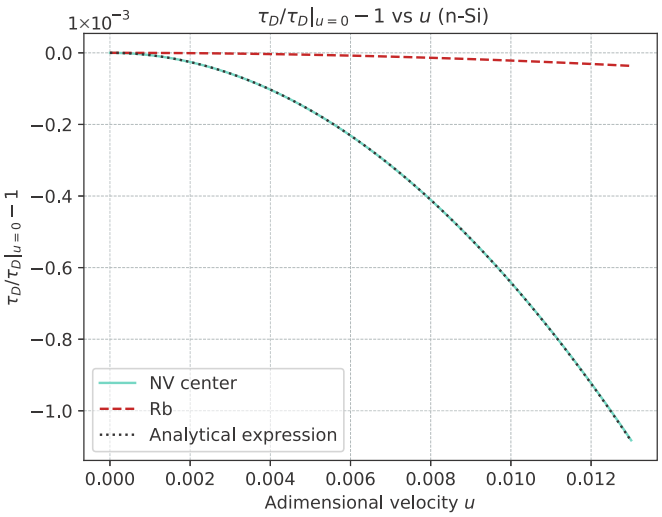

FIG. 4. Decoherence time rate as a function of the adimensional velocity u. The parameter values are $\tilde{\Gamma} = 1$, $\tilde{\Delta}^{\mathrm{NV}} = 0.2$, $\tilde{\Delta}^{\mathrm{Rb}} = 8$, and $r_0/\omega_s = 10^{-2}$.

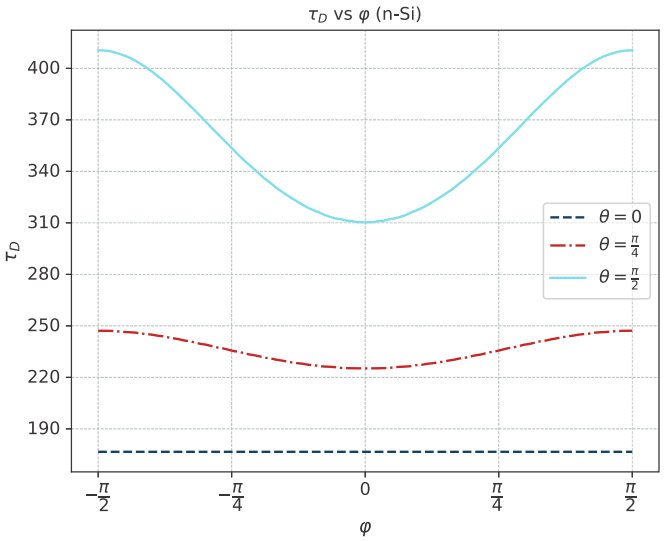

FIG. 5. Decoherence time as a function of the polarization direction of the system. The parameter values are $\tilde{\Gamma} = 1$, $\tilde{\Delta} = 0.2$, $u = 0.3$, and $r_0/\omega_s = 10^{-2}$.

contains two contributions of different nature: (i) a contribution induced by solely vacuum fluctuations (dressed by the presence of the dielectric) and (ii) a contribution induced by the motion of the particle in quantum vacuum. Then it is instructive to study the factor b/a as it constitutes a rate between these two contributions. We define τ_{D} as the net effect of the environment on the particle, while $\tau_{\mathrm{D}}|_{u=0}$ is the decoherence time when the particle is static. If velocity effects are insignificant, $\tau_{\mathrm{D}}/\tau_{\mathrm{D}}|_{u=0} \sim 1$. Hence, by inspecting the rate $(\tau_{\mathrm{D}}/\tau_{\mathrm{D}}|_{u=0} - 1)$ we gain access to b/a. In Fig. 4 this rate is plotted as a function of velocity for two different $\tilde{\Delta}$ values where a quadratic behavior can be easily noted. This behavior is also confirmed by comparing the rate computed by Eq. (12) and the one numerically obtained from the proper definition of τ_{D}.

The difference in the scale factor on each curve reflects how both the net effect of the environment on the particle internal degree of freedom and the contribution derived from the finite velocity are strongly dependent on the parameters of the problem, which are introduced by the material of the half space and the level spacing of the particle and its velocity. For example, the relation b/a takes a numerical value $b/a \sim 6.417$ for a nitrogen-vacancy (NV) center moving over an n-doped silicon (n-Si) surface, while it takes a value $b/a \sim 0.216$ for a rubidium atom moving over the same surface.

The timescale defined in this way inherits also a dependence on the orientation of the polarization of the system $\mathbf{d} = d(\sin(\theta)\cos(\varphi)\hat{x} + \sin(\theta)\sin(\varphi)\hat{y} + \cos(\theta)\hat{z})$ (where φ and θ are the spherical azimuthal and polar angles, respectively) from the coefficients governing the dynamics. Figure 5 shows the φ dependence for different fixed θ values, where it can be seen that the decoherence time is at its smallest value when the polarization is perpendicular to the dielectric surface. If tilted, the coherences fall sooner when the polarization is in the direction of the velocity. This behavior is in accordance with that shown by Intravaia *et al.* in the inset of Fig. 5 in [44], where they have shown the frictional force (computed up to second order in the coupling constant) dependence on the polarization direction. Herein, we find that for the same dipole orientation the force increases and τ_{D} decreases, implying that decoherence effects are stronger in that case. This permits a direct link between decoherence and quantum friction since they exhibit a qualitative inverse proportionality: The stronger the decoherence effect, the stronger the frictional force.

Seeing in Fig. 4 that those variations introduced by the different parameters concerning the material and particle seem to be relevant for the magnitude of the effect, we complete this section by examining some possibilities. For the dielectric material we consider a dielectric to be a gold surface (Au) or an n-doped silicon material (n-Si), gold having the parameters of the Drude-Lorentz model $\omega_s^{\mathrm{Au}} \sim 9.7 \times 10^{15}$ rad/s and $\Gamma/\omega_s \sim 0.003$, while the n-Si parameters are $\Gamma/\omega_s \sim 1$ and $\omega_s^{n\text{-Si}} \sim 2.47 \times 10^{14}$ rad/s. As for the particles (atoms), we consider a Rb atom or a single NV center in diamond as an effective two-level system. In Fig. 6 we show the behavior of $\tau_{\mathrm{D}}/\tau_{\mathrm{D}}|_{u=0} - 1$ in the polarization direction for different sets of frequencies. Therein, we include all four combinations: Dotted lines represent the decoherence time Rb atom and Au, dashed lines correspond to a Rb atom and n-Si, dot-dashed lines correspond to the NV center and Au, and solid lines correspond to the NV center and n-Si. In this way, we can get insight into the importance of the velocity-dependent effects since the bigger the magnitude of the quantity displayed is, the more important the u^2 contribution becomes. The results obtained enhance the idea that the velocity effects induced on the atom depend considerably on the material and particle. The rate between the decoherence timescale at finite velocity and that at null velocity is increased by a factor 10^2 when comparing an NV center moving over an n-Si–coated surface with a Rb atom moving over a gold-coated surface.

We conclude from our analysis that the election of n-Si as the material and an NV center as our system would enhance the effect the most. The NV center consists of a vacancy, or missing carbon atom, in the diamond lattice lying next to a nitrogen atom, which has been substituted for one of the

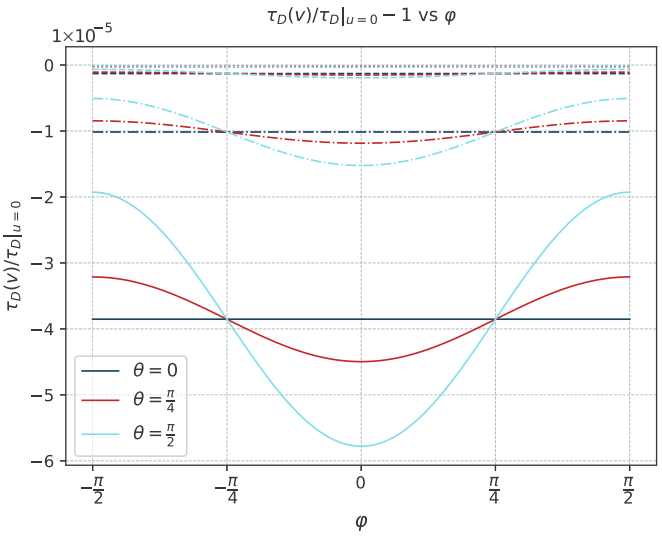

FIG. 6. Decoherence time as a function of the polarization direction of the system, which has polarization $\mathbf{d} = d(\sin(\theta)\cos(\phi)\hat{x} + \sin(\theta)\sin(\phi)\hat{y} + \cos(\theta)\hat{z})$ for both different systems and different materials. Different line styles represent different system-material combinations in this correspondence: Dotted lines correspond to a Rb atom and Au, dashed lines to a Rb atom and n-Si, dot-dashed lines to an NV center and Au, and solid lines to an NV center and n-Si.

carbon atoms. The electron spin is the canonical quantum system and the NV center offers a system in which a single spin can be initialized, coherently controlled, and measured. It is also possible to mechanically move the NV center. For a deeper discussion on the dependence of the effect with the natural level spacing of the system we refer to Appendix B.

V. CONCLUSION

In this article, we have studied the complete dynamics of a two-level system in relative motion with a semi-infinite dielectric material in the electromagnetic vacuum field, with the purpose of characterizing the effects of motion in the dynamics as an alternative to the explicit computation of QF. We have derived the perturbative master equation and obtained the reduced density matrix for all times; we have done this in the near-field regime but otherwise without referring to the Markov approximation. Further, we have obtained an analytical expression in the low-velocity limit when computing the environmental kernels for the vacuum fluctuations.

By a direct inspection of the density matrix evolution, completely different behavior has been found depending on the particle's velocity relative to the dielectric surface. While for low velocities both ρ_{11} and ρ_{12} elements are completely suppressed and the system finally tends to its ground state, when the velocity increases the environmental effect produces mixed asymptotic states, as the element ρ_{11} does not completely vanish but lands at a finite constant value. This divergence on the asymptotic states leads to a completely different behavior of the state purity, which is initially reduced but afterward recovers to unity when the asymptotic state is a pure ground state but is permanently reduced to a lower value when the velocity is high enough as to allow for mix asymptotic states. We conclude this inspection of the state of the two-level system by mentioning that, although for slow enough relative motion there is a preferred time interval in which the effect of velocity can be drawn out from the net vacuum-induced effect, as the velocity is increased and its effect is reflected in the mix asymptotic state, long time studies could supply evidence of the velocity-induced phenomena as well.

From the obtained reduced density matrix, we have estimated the decoherence timescale at which the coherences are strongly suppressed. We have also provided a low-velocity expression for this timescale, which has been shown to scale as u^2 in accordance with previous results, and we have further analyzed its dependence on a variety of parameters involved in the dynamics. Through analytic considerations, we have shown how both the net effect of the composite environment on the particle and the velocity-dependent effect are strongly dependent on the material parameters and the system level spacing, allowing us to amplify or weaken the magnitude by a sensible choice.

Finally, as for the dependence upon the polarization direction, we have found results for the decoherence time in agreement with those existing in the literature for quantum friction, showing a qualitative inverse proportionality among them and the frictional force. This means that a link between the decoherence time and the quantum frictional force can be established since noncontact friction seems to enhance the decoherence of the moving atom. This suggests that measuring decoherence times could be used to indirectly demonstrate the existence of quantum friction. Furthermore, we have analyzed the different compositions of the material and effective two-level system that can be useful in experimental setups with the purpose of enhancing the effect of the finite velocity on the internal degree of the particle. In particular, we found the rate between the decoherence timescale at finite velocity and that at null velocity to be bigger by a factor 10^2 when comparing an NV center moving over an n-Si surface with a Rb atom moving over a gold surface. We are confident that our work can spark renewed optimism in the design of new experimental setups for the detection of noncontact friction with the hope that this nonequilibrium phenomenon can be viewed in measurable reality soon.

ACKNOWLEDGMENTS

This work was supported by ANPCyT, CONICET, and Universidad de Buenos Aires, Argentina.

APPENDIX A: MASTER-EQUATION COEFFICIENTS

The polarization vector of the particle can be split into a module and direction as $\mathbf{d} = d(n_x\check{x} + n_y\check{y} + n_z\check{z})$, with $\sum n_i^2 = 1$. Then the coefficients $D(v,t)$, $f(v,t)$, and $\zeta(v,t)$ appearing in the master equation are given, in polar coordinates for the parallel wave vector $\mathbf{k}$, by expressions of the form

$$N(v,t) = \frac{d^2}{4\pi^2\hbar}\int_0^t dt' \int_0^{2\pi} d\theta_k \int_0^\infty k^2 dk\, d\omega\, e^{-2ak} \times \left\{[n_x\cos(\theta_k) + n_y\sin(\theta_k)]^2 + n_z^2\right\}$$

$$\times \frac{\Gamma\omega_p^2\,\omega}{\left(\omega^2-\omega_s^2\right)^2+\Gamma^2\omega^2}$$
$$\times \mathrm{trig}[\Delta(t-t')]\mathrm{trig}[(\omega-ikv\cos\theta_k)(t-t')],$$

where we are referring to any of the coefficient functions as $N(v,t)$ and either function $\sin(x)$ or $\cos(x)$ as trig.

Expressing the trigonometric function $\mathrm{trig}[(\omega - ikv\cos\theta_k)(t-t')]$ in terms of exponential functions, the integral over k can be performed directly

$$\int_0^\infty k^2 e^{-2ak} e^{\pm ikv\cos(\theta)(t-t')}dk = \frac{2}{[2a\mp iv\cos(\theta)(t-t')]^3},$$

as well as the nonzero integrals over θ_k,

$$\int_0^{2\pi} d\theta \frac{\cos^2\theta}{[2a\pm iv\cos(\theta)(t-t')]^3} = \frac{2\pi[2a^2-v^2(t-t')^2]}{[4a^2+v^2(t-t')^2]^{5/2}}$$
$$\times \int_0^{2\pi} d\theta \frac{\sin^2\theta}{[2a\pm iv\cos(\theta)(t-t')]^3} = \frac{\pi}{[4a^2+v^2(t-t')^2]^{3/2}}$$
$$\times \int_0^{2\pi} d\theta \frac{1}{[2a\pm iv\cos(\theta)(t-t')]^3} = \frac{\pi[8a^2-v^2(t-t')^2]}{[4a^2+v^2(t-t')^2]^{5/2}}.$$

Then, if we define dimensionless parameters

$$u=\frac{v}{\omega_s\times a},\quad \tilde{\Delta}=\frac{\Delta}{\omega_s},\quad \tilde{\Gamma}=\frac{\Gamma}{\omega_s}, \tag{A1}$$

the dimensional coefficient $r_0 = d^2\omega_p^2/\hbar\omega_s^2 a^3$, and change to dimensionless variables

$$\frac{\omega}{\omega_s}\to\omega,\quad \frac{\Gamma}{\omega_s}\to t, \tag{A2}$$

the functions can be written as

$$D(v,t)=\frac{r_0}{2\pi}\int_0^t dt'\int_0^\infty d\omega\frac{\tilde{\Gamma}\omega}{(\omega^2-1)^2+\tilde{\Gamma}^2\omega^2}\cos(\tilde{\Delta}t')\cos(\omega t')\mathbf{P}(ut'), \tag{A3}$$
$$f(v,t)=\frac{r_0}{2\pi}\int_0^t dt'\int_0^\infty d\omega\frac{\tilde{\Gamma}\omega}{(\omega^2-1)^2+\tilde{\Gamma}^2\omega^2}\sin(\tilde{\Delta}t')\cos(\omega t')\mathbf{P}(ut'), \tag{A4}$$
$$\zeta(v,t)=\frac{r_0}{2\pi}\int_0^t dt'\int_0^\infty d\omega\frac{\tilde{\Gamma}\omega}{(\omega^2-1)^2+\tilde{\Gamma}^2\omega^2}\sin(\tilde{\Delta}t')\sin(\omega t')\mathbf{P}(ut'), \tag{A5}$$

where $\mathbf{P}(ut')$ is an algebraic function given by

$$\mathbf{P}(ut')=2n_x^2\frac{2-u^2t'^2}{(4+u^2t'^2)^{5/2}} + \frac{n_y^2}{(4+u^2t'^2)^{3/2}}+n_z^2\frac{(8-u^2t'^2)}{(4+u^2t'^2)^{5/2}}. \tag{A6}$$

In the following, we will consider only $D(v,t)$, since the other coefficients can be treated in a very similar manner. The expression to be integrated over ω,

$$\frac{1}{2}\int_0^\infty d\omega\frac{\tilde{\Gamma}\omega}{(\omega^2-1)^2+\tilde{\Gamma}^2\omega^2}(e^{i\omega t'}+e^{-i\omega t'}), \tag{A7}$$

is holomorphic everywhere but on the poles given by the roots of the denominator $\{\tilde{\omega}_r, -\tilde{\omega}_r, \text{c.c.}\}$, with

$$\tilde{\omega}_r=\frac{1}{\sqrt{2}}\sqrt{2-\tilde{\Gamma}+i\sqrt{4-\tilde{\Gamma}}}. \tag{A8}$$

For $\tilde{\Gamma}$ values satisfying $\tilde{\Gamma}<2$ these are complex poles with both real and imaginary nonvanishing parts, while for $\tilde{\Gamma}>2$, $\tilde{\omega}_r$ is purely imaginary. The integral in (A7) can be expressed in terms of exponential integral functions as

$$\frac{1}{4\sqrt{4-\tilde{\Gamma}^2}}[\pi e^{i\omega_r t}-ie^{i\omega_r t}E_1(i\omega_r t)-ie^{-i\omega_r t}E_1(-i\omega_r t)+\text{c.c.}], \tag{A9}$$

where the terms containing the functions E_1 are negligible when compared to the exponential term as long as $\tilde{\Gamma}\ll 1$ but cease to be negligible for $\tilde{\Gamma}\sim 1$.

First, we will focus on the approximated result obtained for low $\tilde{\Gamma}$ values (i.e., disregarding all terms containing E_1 functions) to explain how we have considered the correction introduced by them at the end of this Appendix. At this point, we are only left with the time integral to be addressed. In order to do so, we will extend t' to the complex plane and modify the integration path conveniently (Fig. 7). By observing that for nonrelativistic velocities of the particle, oscillations in

$$D(v,t)=\frac{r_0}{4\pi}\frac{\pi}{\sqrt{4-\tilde{\Gamma}^2}} \times\int_0^t dt'(e^{i(\tilde{\omega}_r+\tilde{\Delta})t'}+e^{i(\tilde{\omega}_r-\tilde{\Delta})t'}+\text{c.c.})\mathbf{P}(ut') \tag{A10}$$

occur on a much faster timescale than $\mathbf{P}(ut')$ variation, we can adopt the steepest-descent method to replace the integrals over

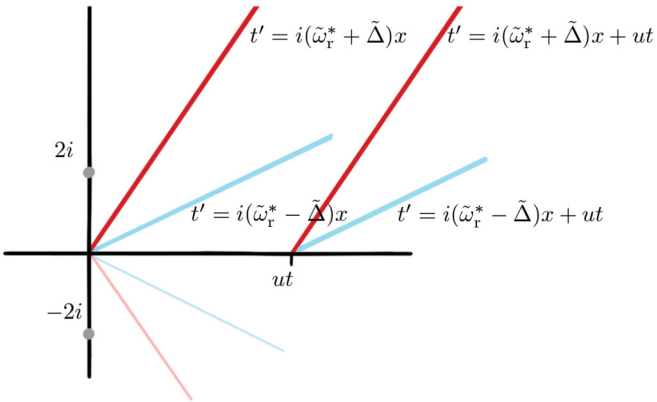

FIG. 7. Constant phase contours for an integral over the variable t' which was extended to the complex plane.

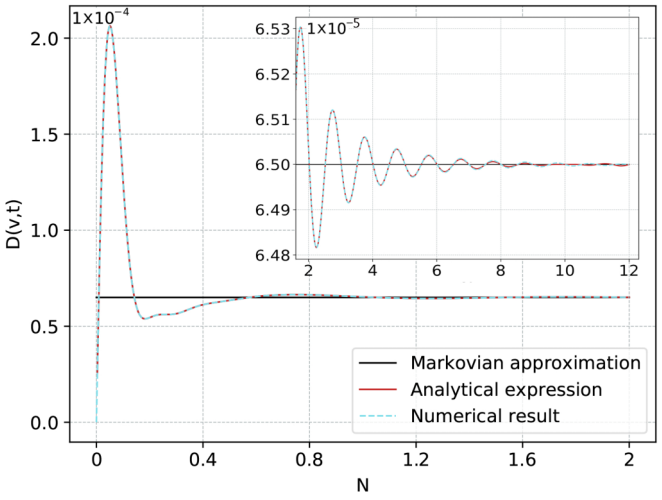

FIG. 8. Coefficient $D(v,t)$ evolution in natural cycles $N = \frac{t}{2\pi/\tilde{\Delta}}$, comparing the analytical expression, the numerical result, and the value obtained when performing a Markov approximation. The parameter values are $a = 5$ nm, $\tilde{\Gamma} = 1$, $\tilde{\Delta} = 0.2$, $u = 0.003$, and $\mathbf{d} = d(1,0,0)$.

the real axis intervals by integrals along a constant phase path for each exponential.

Over these paths, the integral is dominated by the contributions at those points where the exponent is a local maximum, allowing for an expansion of the algebraic function in the parameter of the curve. Following this method, we get, up to second order in the adimensional velocity u, the approximated expression

$$D(v,t) \sim \frac{r_0}{8}\frac{1}{\sqrt{4-\tilde{\Gamma}^2}} \times \left[-\frac{d^{(i)}}{8}\mathrm{Im}\frac{1}{\tilde{\omega}_\mathrm{r}+\tilde{\Delta}} - \frac{3}{32}d^{(a)}u^2\mathrm{Im}\frac{1}{(\tilde{\omega}_\mathrm{r}+\tilde{\Delta})^3} + \mathbf{P}(ut')\mathrm{Im}\frac{e^{i(\tilde{\omega}_\mathrm{r}+\tilde{\Delta})t'}}{\tilde{\omega}_\mathrm{r}+\tilde{\Delta}} + 12\mathbf{R}(ut)u^2\mathrm{Im}\frac{e^{i(\tilde{\omega}_\mathrm{r}+\tilde{\Delta})t'}}{(\tilde{\omega}_\mathrm{r}+\tilde{\Delta})^3} - 3\mathbf{Q}(ut)tu^2\mathrm{Re}\frac{e^{i(\tilde{\omega}_\mathrm{r}+\tilde{\Delta})t'}}{(\tilde{\omega}_\mathrm{r}+\tilde{\Delta})^2}\right] + (\tilde{\Delta}\leftrightarrow-\tilde{\Delta}), \tag{A11}$$

where $d^{(i)} = 1 + n_z^2$ and $d^{(a)} = 3n_x^2 + n_y^2 + 4n_z^2$. The additional algebraic functions $\mathbf{Q}$ and $\mathbf{R}$ appearing in this expression for $D(v,t)$ are given by

$$\mathbf{Q} = 2\frac{6-u^2t^2}{(4+u^2t^2)^{7/2}}n_x^2 + \frac{n_y^2}{(4+u^2t^2)^{5/2}} + \frac{16-u^2t^2}{(4+u^2t^2)^{7/2}}n_z^2,$$

$$\mathbf{R} = 2\frac{(6-u^2t^2)^2-30}{(4+u^2t^2)^{9/2}}n_x^2 + \frac{(1-u^2t^2)}{(4+u^2t^2)^{7/2}}n_y^2 + \frac{16-27u^2t^2+u^4t^4}{(4+u^2t^2)^{9/2}}n_z^2,$$

while approximate solutions can be found for $f(v,t)$ and $\zeta(v,t)$, following an analogous procedure.

In order to incorporate a correction that allows us to investigate greater $\tilde{\Gamma}$ values, we expand $\mathbf{P}(ut)$ up to second order in

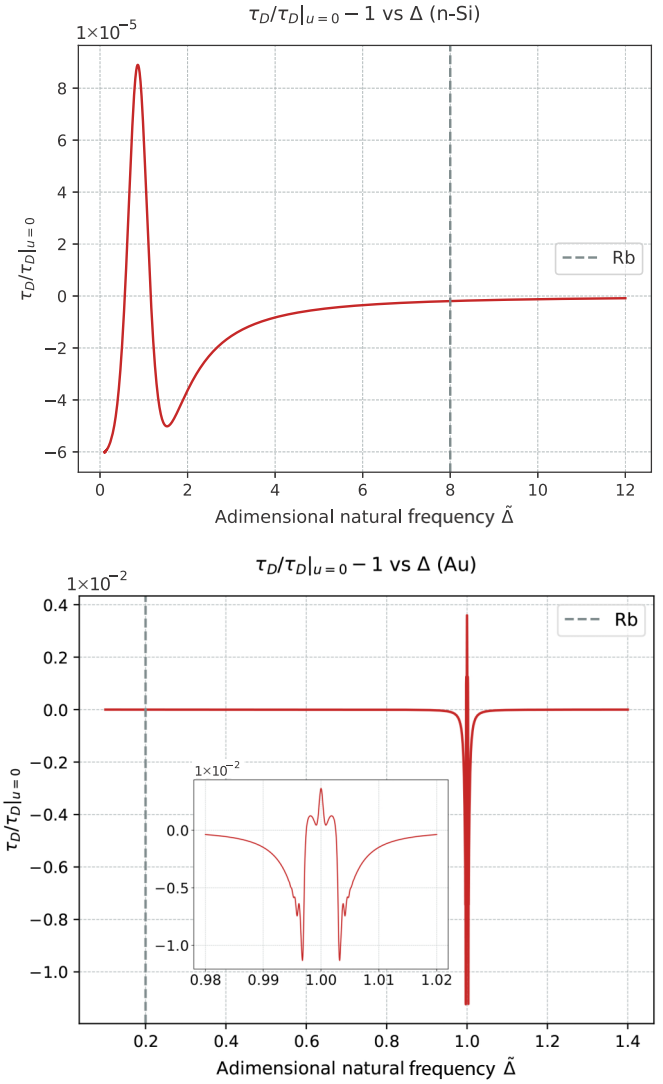

FIG. 9. Decoherence time as a function of the dimensionless level spacing $\tilde{\Delta}$ of the system, normalized with the null velocity value, considering an n-Si (up) and a gold (down) dielectric. The parameter values are $\tilde{\Gamma} = 1$ and $u = 0.003$ for n-Si and $\tilde{\Gamma} = 3\times10^{-3}$, $u = 1.5\times10^{-4}$, and $\mathbf{d} = d(1,0,0)$ for Au.

u in the integrand so that

$$\mathbf{P}(ut') \sim \frac{d^{(i)}}{8} - \frac{3}{64}d^{(a)}u^2t'^2. \tag{A12}$$

This allows us to write the remaining part of the integral as

$$\Delta D(v,t) = \frac{r_0}{16\pi}\frac{1}{\sqrt{4-\tilde{\Gamma}^2}}\left[\frac{d^{(i)}}{8} + \frac{3}{64}d^{(a)}u^2\partial_{\tilde{\Delta}}^2\right] \times \int_0^t dt'\,\{(-i)(e^{i(\omega_\mathrm{r}+\tilde{\Delta})t}E_1(i\omega_\mathrm{r}t) + e^{-i(\omega_\mathrm{r}+\tilde{\Delta})t}E_1(-i\omega_\mathrm{r}t)) + \mathrm{c.c.}\} + (\tilde{\Delta}\leftrightarrow-\tilde{\Delta}). \tag{A13}$$

This integral can be formally solved to

$$\Delta D(v,t) = \frac{r_0}{16\pi}\frac{1}{\sqrt{4-\tilde{\Gamma}^2}}\left[\frac{d^{(i)}}{8}+\frac{3}{64}d^{(a)}\,u^2\partial_{\tilde{\Delta}}^2\right] \times\left\{\frac{-2\pi i}{\tilde{\omega}_r+\tilde{\Delta}}+\left[[E_1(-i\tilde{\Delta}t)-E_1(i\tilde{\Delta}t)]\frac{1}{\tilde{\omega}_r+\tilde{\Delta}}\right.\right. - \frac{e^{i(\omega_r+\tilde{\Delta})t}}{\tilde{\omega}_r+\tilde{\Delta}}E_1(i\omega_r t)+\frac{e^{-i(\omega_r+\tilde{\Delta})t}}{\tilde{\omega}_r+\tilde{\Delta}}E_1(-i\omega_r t) \left.\left.+(\tilde{\Delta}\leftrightarrow-\tilde{\Delta})\right]+\text{c.c.}\right\}. \tag{A14}$$

These expressions have been tested against the numerical results. It is easy to obtain a comparison from Fig. 8, where the evolution of $D(v,t)$ is plotted for $\tilde{\Gamma}=1$. The dashed line representing the numerical result is not distinguishable from the red solid line representing the analytical expression. Both the numerical and the analytical results tend to their Markovian approximation values for a few cycles for these parameter values, but a difference between the values obtained when computing $\int D(v,t)$ and $D^{\text{Markov}}t$ can be suspected.

APPENDIX B: DEPENDENCE ON LEVEL SPACING

As suggested in Sec. IV, the strength of the velocity-dependent effect can be studied from the relation between the decoherence time defined by Eq. (12) for finite and zero velocities. Exploring the dependence of this relation on the level spacing of the atom, it can be seen in Fig. 9 that an appropriate choice of the particle to be considered can enhance (or diminished) considerably the effect of velocity. Rigorously speaking, the dependence is not on the level spacing alone but on the relation between the Drude-Lorentz parameters of the material and the level spacing. It can be seen that, moving away from the prohibited near-resonance range, the difference between the vacuum and velocity effects is maximum for certain values of natural level spacing $\tilde{\Delta}$, approaching zero sufficiently far from resonance. In order to maximize the effect to be studied, we consider the system to be an NV center of natural frequency $\tilde{\Delta}=0.2$ moving over an n-doped silicon surface or an NV center of natural frequency $\tilde{\Delta}=0.9$ moving over a gold surface unless explicitly indicated.

[1] H. B. G. Casimir, Proc. K. Ned. Akad. Wet. **51**, 793 (1948).
[2] P. W. Milonni, *The Quantum Vacuum: An Introduction to Quantum Electrodynamics* (Academic, New York, 2013).
[3] S. K. Lamoreaux, Phys. Rev. Lett. **78**, 5 (1997).
[4] M. Bordag, G. Klimchitskaya, U. Mohideen, and V. Mostepanenko, *Advances in the Casimir Effect* (Oxford University Press, Oxford, 2009), Vol. 145.
[5] M. Bordag, U. Mohideen, and V. Mostepanenko, Phys. Rep. **353**, 1 (2001).
[6] K. A. Milton, *The Casimir Effect: Physical Manifestations of Zero-Point Energy* (World Scientific, Singapore, 2001).
[7] K. A. Milton, J. Phys. A: Math. Gen. **37**, R209 (2004).
[8] S. Reynaud, A. Lambrecht, C. Genet, and M. T. Jaekel, C. R. Acad. Sci. Paris Ser. **IV-2**, 1287 (2001).
[9] D. A. Dalvit, P. A. M. Neto, and F. D. Mazzitelli, Lect. Notes Phys. **834**, 419 (2011).
[10] P. D. Nation, J. R. Johansson, M. P. Blencowe, and F. Nori, Rev. Mod. Phys. **84**, 1 (2012).
[11] C. M. Wilson, G. Johansson, A. Pourkabirian, M. Simoen, J. R. Johansson, T. Duty, F. Nori, and P. Delsing, Nature (London) **479**, 376 (2011).
[12] P. Lähteenmäki, G. Paraoanu, J. Hassel, and P. J. Hakonen, Proc. Natl. Acad. Sci. U.S.A. **110**, 4234 (2013).
[13] J. B. Pendry, J. Phys.: Condens. Matter **9**, 10301 (1997).
[14] J. B. Pendry, New J. Phys. **12**, 033028 (2010).
[15] J. B. Pendry, New J. Phys. **12**, 068002 (2010).
[16] U. Leonhardt, New J. Phys. **12**, 068001 (2010).
[17] T. Philbin and U. Leonhardt, New J. Phys. **11**, 033035 (2009).
[18] A. I. Volokitin and B. N. J. Persson, Rev. Mod. Phys. **79**, 1291 (2007).
[19] J. Klatt, M. B. Farías, D. A. R. Dalvit, and S. Y. Buhmann, Phys. Rev. A **95**, 052510 (2017).
[20] G. Barton, New J. Phys. **12**, 113045 (2010).
[21] F. Intravaia, V. E. Mkrtchian, S. Y. Buhmann, S. Scheel, D. A. R. Dalvit, and C. Henkel, J. Phys.: Condens. Matter **27**, 214020 (2015).
[22] S. Scheel and S. Y. Buhmann, Phys. Rev. A **80**, 042902 (2009).
[23] F. Intravaia, R. O. Behunin, and D. A. R. Dalvit, Phys. Rev. A **89**, 050101(R) (2014).
[24] D. Reiche, F. Intravaia, J.-T. Hsiang, K. Busch, and B. L. Hu, Phys. Rev. A **102**, 050203(R) (2020).
[25] M. B. Farias, W. J. M. Kort-Kamp, and D. A. R. Dalvit, Phys. Rev. B **97**, 161407(R) (2018).
[26] J. Marino, A. Recati, and I. Carusotto, Phys. Rev. Lett. **118**, 045301 (2017).
[27] F. Intravaia, M. Oelschläger, D. Reiche, D. A. R. Dalvit, and K. Busch, Phys. Rev. Lett. **123**, 120401 (2019).
[28] M. B. Farias, C. D. Fosco, F. C. Lombardo, and F. D. Mazzitelli, Phys. Rev. D **95**, 065012 (2017).
[29] M. Belén Farías, C. D. Fosco, F. C. Lombardo, F. D. Mazzitelli, and A. E. Rubio López, Phys. Rev. D **91**, 105020 (2015).
[30] L. Viotti, M. Belén Farías, P. I. Villar, and F. C. Lombardo, Phys. Rev. D **99**, 105005 (2019).
[31] A. I. Volokitin and B. N. J. Persson, Phys. Rev. Lett. **106**, 094502 (2011).
[32] A. I. Volokitin, Phys. Rev. B **94**, 235450 (2016).
[33] J. Klatt, R. Bennett, and S. Y. Buhmann, Phys. Rev. A **94**, 063803 (2016).
[34] M. B. Farías and F. C. Lombardo, Phys. Rev. D **93**, 065035 (2016).
[35] M. B. Faras, F. C. Lombardo, A. Soba, P. I. Villar, and R. S. Decca, npj Quantum Inf. **6**, 25 (2020).
[36] G. Barton, Proc. R. Soc. London Ser. A **453**, 2461 (1997).
[37] G. Barton, Rep. Prog. Phys. **42**, 963 (1979).
[38] H.-P. Breuer and F. Petruccione, *The Theory of Open Quantum Systems* (Oxford University Press, Oxford, 2002).

[39] J. P. Paz and W. H. Zurek, in *Coherent Atomic Matter Waves*, edited by R. Kaiser, C. Westbrook, and F. David (Springer, Berlin, 2001), pp. 533–614.

[40] A. J. Leggett, S. Chakravarty, A. T. Dorsey, M. P. A. Fisher, A. Garg, and W. Zwerger, Rev. Mod. Phys. **59**, 1 (1987).

[41] S. Dattagupta and S. Puri, *Dissipative Phenomena in Condensed Matter: Some Applications*, Springer Series in Materials Science Vol. 71 (Springer, Berlin, 2004).

[42] C. Fleming, N. I. Cummings, C. Anastopoulos, and B. L. Hu, J. Phys. A: Math. Theor. **43**, 405304 (2010).

[43] P. Haikka and S. Maniscalco, Phys. Rev. A **81**, 052103 (2010).

[44] F. Intravaia, R. O. Behunin, C. Henkel, K. Busch, and D. A. R. Dalvit, Phys. Rev. A **94**, 042114 (2016).

[45] A. A. Svidzinsky, Phys. Rev. Res. **1**, 033027 (2019).

[46] M. F. Maghrebi, R. Golestanian, and M. Kardar, Phys. Rev. A **88**, 042509 (2013).